Anti-CD206 antibody-conjugated Fe_3O_4-based PLGA nanoparticles selectively promote tumor-associated macrophages to polarize to the pro-inflammatory subtype

YUN ZHOU[1*], KE-TING QUE[2*], HUA-MING TANG[1], PENG ZHANG[1], QIAN-MEI FU[1] and ZUO-JIN LIU[2]

[1]Department of Cardiothoracic Surgery and Abdominal Hernia Surgery, The People's Hospital of Kai Zhou District; [2]Department of Hepatobiliary Surgery, The Second Affiliated Hospital of Chongqing Medical University, Chongqing 400000, P.R. China

Received February 25, 2020; Accepted September 1, 2020

DOI: 10.3892/ol.2020.12161

Abstract. M2 macrophages serve roles in inhibiting inflammation and promoting tumor development. Reversing tumor-associated macrophages (TAMs) from M2- to M1-type polarization may provide an important strategy for tumor immunotherapy. The present study aimed to enhance antitumor immunity by targeting the concentration of iron in macrophages. Fe_3O_4-based poly(lactic-co-glycolic) acid (PLGA) nanoparticles surface-modified with an anti-CD206 monoclonal antibody were prepared using the oil in water single-emulsion technique. Particle size was measured using a particle size analyzer, the ζ potential was determined using a ζ potential analyzer and the carrier rate of Fe_3O_4 was measured using an iron assay kit. The conjugation of anti-CD206, and the ability to target M2 macrophages were studied via immunofluorescence. Polarization indexes of the macrophages were detected using both western blotting and reverse transcription-quantitative PCR (RT-qPCR), and a mouse model with subcutaneous tumors was established to verify the antitumor effects of the nanoparticles *in vivo*. Nanoparticles had a mean diameter in the range of 260-295 nm, and the ζ potential values were between -19 and -33 mV. The Fe_3O_4 association efficiency ranged from 65-75%, whereas the anti-CD206 conjunction efficiency ranged from 65-70%. The immunofluorescence experiments were able to demonstrate the successful targeting of the M2 macrophages. The western blotting and RT-qPCR experiments identified that CD206-Fe_3O_4-PLGA and Fe_3O_4-PLGA promoted the expression of TNF-α, inducible nitric oxide synthase (iNOS) and IL-1β in the macrophages. The *in vivo* studies indicated that CD206-Fe_3O_4-PLGA nanoparticles were able to promote CD86 expression in TAMs, with CD86 being a specific marker of the M1 subtype. In summary, nanoparticles were characterized in the present study by their mean particle size, polydispersity index, ζ potential and morphology, as well as by their association with Fe_3O_4 and conjugation with the anti-CD206 monoclonal antibody. Collectively, the present results suggested that the nanoparticles were able to both target M2 macrophages and reverse the M2 polarization of the macrophages to the M1 phenotype via the release of coated iron-oxide particles.

Correspondence to: Professor Zuo-Jin Liu, Department of Hepatobiliary Surgery, The Second Affiliated Hospital of Chongqing Medical University, 76 Linjiang Road, Chongqing 400000, P.R. China
E-mail: liuzuojin66@hotmail.com

*Contributed equally

Key words: iron oxide nanoparticle, poly(lactic-co-glycolic) acid, targeted drug delivery, tumor immunotherapy

Introduction

Different macrophage subtypes have varying surface molecules and secrete different cytokines. M1 macrophages secrete pro-inflammatory factors, including TNF-α, IL-23 and IL-1β, which exert pro-inflammatory and cytotoxic effects in the early stage of the inflammatory response (1). On the other hand, M2 macrophages secrete IL-10, which promotes angiogenesis and is involved in the pathological processes of tissue repair and wound healing (1). Macrophages also exert important roles in iron metabolism due to their versatile roles during innate immunity. For instance, M1 macrophages are often referred to as an 'iron-sequestering phenotype'. These M1 macrophages express high levels of ferritin, divalent metal transporter 1 and CD91, but low levels of transferrin receptor and ferroportin (FPN) (2). Moreover, M1 macrophages restrict the growth and proliferation of pathogens by maximizing iron uptake and storage, lowering iron excretion and decreasing the levels of iron ions available to pathogens (3,4). M2 have an iron-release phenotype, and thus can express more FPN and release intracellular iron ions (3-5). M2 macrophages release iron ions from the labile iron pool, alter the local microenvironment and increase the availability of iron ions in adjacent cells, thereby promoting the proliferation of adjacent cells, increasing collagen deposition and accelerating damage repair and regeneration (5).

Fe_3O_4 nanoparticles are commonly used as contrast agents and drug carriers (6,7). Zanganeh *et al* (8) reported that Fe_3O_4 nanoparticles could promote the polarization of tumor-associated macrophages (TAMs) towards the M1 type, and significantly increase the production of reactive oxygen species (ROS) in macrophages. Super paramagnetic iron-oxide nanoparticles (SPIONs) are mainly phagocytized by macrophages, and are degraded into iron ions in lysosomes (9), causing iron overload in macrophages and ultimately promoting the repolarization of M2 macrophages to M1 macrophages (10).

Poly(lactic-co-glycolic) acid (PLGA) is a type of polymer synthesized by the polymerization of lactic acid and glycolic acid in a certain ratio (11). Copolymers with different degradation periods can be obtained by adjusting the ratio and molecular weight of the two polymers. The final metabolic products of PLGA in the body are water and carbon dioxide, and therefore it is safe to use and is non-toxic (12). PLGA, first used as a long-acting controlled-release system in the 1970s, has been certified by the US Food and Drug Administration, and is officially included in the US Pharmacopoeia as a pharmaceutical excipient (13,14). Currently, numerous studies have focused on PLGA as a targeted nano-delivery system for delivering chemotherapeutic cancer drugs to the target tissues (15). PLGA offers a number of advantages, including decreased systemic toxicity, increased blood circulation times and enhanced accumulation at the tumor site for the delivered drug (16-19). Therapeutic nanoparticles can be rapidly removed from the internal circulation by phagocytic immune cells, mainly by the circulating monocytes and macrophages (20). Previous studies have revealed that the majority of the nanoparticles concentrate in the liver and spleen, and only a small portion of the nanoparticles are deposited in tumor tissues via the blood circulation (21,22).

Targeted ligands, such as antibodies and aptamers, are often bound to the outer surface of nanoparticles during the process of designing 'active' drug delivery systems, which helps to deliver payloads specifically to the sites carrying homologous receptors for targeted ligands (23). Ligands help to internalize conjugates, and the payload carried by conjugates can be transferred in cells (23-25).

The present study aimed to enhance antitumor immunity by targeting the iron concentration in TAMs using Fe_3O_4-based PLGA nanoparticles, which were conjugated with anti-CD206 monoclonal antibody.

Materials and methods

Materials. Acid-terminated PLGA copolymer (50:50 ratio of lactic acid to glycolic acid; molecular weight, 12 kDa) was purchased from Sigma-Aldrich; Merck KGaA. Fe_3O_4 nanocrystals (diameter, 10 nm) coated with oleic acid and dispersed in chloroform (20 mg/ml) were provided by Xi'an Ruixi Biological Technology Co., Ltd. 2-Morpholinoethanesulfonic acid (MES), 1-ethyl-3-(3-dimethylaminopropyl) carbodiimide hydrochloride (EDC) and *N*-hydroxysuccinimide (NHS) were purchased from Sigma-Aldrich; Merck KGaA. Ferric citrate was also obtained from Sigma-Aldrich; Merck KGaA. Invitrogen® FBS was purchased from Thermo Fisher Scientific, Inc., while HyClone® DMEM was obtained from Cytiva. Penicillin and Fungizone® antimycotic and DMSO were provided by Thermo Fisher Scientific, Inc.

GAPDH (cat. no. ab9485), anti-CD206 (cat. no. ab64693), F4/80 (cat. no. ab100790) and CD86 (cat. no. ab119857) monoclonal antibodies were obtained from Abcam. IL-1β (cat. no. GTX74034), IL-10 (cat. no. GTX130513), TGF-β (cat. no. GTX21279), TNF-α (cat. no. GTX110520), inducible nitric oxide synthase (iNOS; cat. no. GTX130246) and Arginase 1 (Arg1; cat. no. GTX124113) were purchased from GeneTex, Inc. Goat anti-rabbit secondary antibodies labeled with Alexa Fluor® 647 (cat. no. ab150079), rat anti-mouse secondary antibodies labeled with FITC (cat. no. ab99572) and goat anti-rabbit secondary antibodies labeled with tetramethylrhodamine (TRITC; cat. no. ab7087) were obtained from Abcam. Horseradish peroxidase-labeled goat anti-mouse (cat. no. A0216) and goat anti-rabbit (cat. no. A0208) secondary antibodies were purchased from Beyotime Institute of Biotechnology.

The iron ion detection kit was purchased from Sigma-Aldrich; Merck KGaA. BSA, DilC18(3) (DIL) and poly (vinyl alcohol) (PVA) were obtained from Beyotime Institute of Biotechnology. The primers used in the PCR experiments were from BBI Life Sciences Corporation, and the sequences of these PCR primers are presented in Table I.

Preparation of nanoparticles. The oil in water method (26) was used to manufacture the nanoparticles. PLGA (200 mg), Fe_3O_4 (400 μl of a 20 mg/ml solution) and 9.4 μg DIL were dissolved in 2 ml dichloromethane at room temperature for 30 sec as the oil phase, and then 8 ml 4% PVA solution was added to serve as the aqueous phase. The emulsion formed was homogenized at room temperature using an ultrasonic oscillation instrument (Shanghai Yanyong Ultrasonic Instrument Co., Ltd.) with the amplitude set at 70% for 1 min. The previous emulsion was subsequently added to 15 ml 0.2% PVA aqueous solution, and the organic solvent was removed via evaporation using a rotavapor for 90 min at room temperature. This was followed by a subsequent centrifugation (15,000 x g for 10 min at 4˚C) to obtain the nanoparticles, which were then washed three times with water.

Conjugation of anti-CD206 antibody to the nanoparticles. Carbodiimide-mediated amide bond formation was used to prepare the anti-CD206 monoclonal antibody-conjugated nanoparticles, as described previously by Moura *et al* (27). The prepared nanoparticles were resuspended in 10 ml MES buffer (pH 6.0). A total of 1 ml EDC (0.1 M) was added to the nanoparticle suspension with mild stirring for 15 min at room temperature, then 1 ml NHS (0.7 M) was added and the mixture was continually stirred for a further 45 min. The remaining reagents in the coupling reaction were removed via centrifugation (15,000 x g for 10 min at 4˚C). Subsequently, the nanoparticles were washed with MES (pH 8.0) for 5 min and repeat three times, and finally re-dispersed in 2 ml double-distilled water. Anti-CD206 antibody solution (100 μl) was added to the activated nanoparticle suspension for antibody conjugation, and incubated at room temperature for 2 h. The mixture was centrifuged again (15,000 x g for 10 min at 4˚C) in order to remove any excess unconjugated anti-CD206 antibody, and washed three times with PBS for 5 min.

Table I. Sequences of the primers used for reverse transcription-quantitative PCR.

Primer	Forward	Reverse
Arg1	5'-CCCCAGTACCAACAGGACTACC-3'	5'-TGAACGTGGCGGAATTTTGT-3'
TNF-α	5'-GGATCTCAAAGACAACCAAC-3'	5'-ACAGAGCAATGACTCCAAAG-3'
iNOS	5'-CTGCAGCACTTGGATCAGGAACCTG-3'	5'-GGAGTAGCCTGTGTGCACCTGGAA-3'
TGF-β	5'-ACCTGCAAGACCATCGACAT-3'	5'-GGTTTTCTCATAGATGGCGT-3'
GAPDH	5'-CACCCACTCCTCCACCTTTG-3'	5'-CCACCACCCTGTTGCTGTAG-3'

Arg1, arginase-1; iNOS, inducible nitric oxide synthase.

Measurements of nanoparticles. The particle size, size distribution (polydispersity index) and ζ potential of the nanoparticles produced were measured using a laser particle size analyzer (Brookhaven Instruments Corporation). Using ultrapure water as the medium, 50 mg nanoparticles were distributed in ultrapure water and a 2 ml suspension was then collected and placed in the colorimetric dish. When the temperature of suspension had equilibrated at 25˚C, the distribution and particle size of the microspheres were analyzed using a laser particle size analyzer. The nanoparticle freeze-dried powder was adhered to the electron microscope plate with conductive adhesive, and the surface characteristics of the sample were observed at room temperature by scanning using an electron microscope (S-3000N model; Hitachi, Ltd., magnification, x50,000). All samples were measured with three independent batch power sources (six runs; 10 cycles each). Suspensions were prepared using 50 mg nanoparticle freeze-dried 173 powder dispersed in ultra9pure water, and then 2 ml suspension was used to observe and collect images with an optical microscope (LV100ND; Nikon instruments Co., Ltd, magnification, x100).

Tissue immunofluorescence. The frozen sections of subcutaneous tumor tissue (thickness, 5 μm) were prepared at -16˚C and preserved at -4˚C, and the sections were washed three times with PBS and sealed at room temperature for 1 h with 2% BSA. The sections were subsequently washed three times with PBS and incubated with primary antibodies of F4/80 (1:1,000) and CD86 (1:1,000) at room temperature for 12 h. Next, the frozen sections were washed with PBS and incubated with secondary antibodies (cat. nos. ab150079 and ab99572; 1:1,000) at room temperature for 1 h. DAPI was used for nuclear staining at room temperature for 5 min, and the tissue sections were sealed via anti-fluorescent quenching. Under high-power magnification (x200), tissue immunofluorescence micrographs were screened, and images were captured using a fluorescence microscope (Leica Microsystems, Inc.).

ROS level detection. Macrophages were cultured in 2 ml medium with 500 μl suspension of PLGA (10 mg), Fe_3O_4-PLGA (10 mg) or CD206-Fe_3O_4-PLGA (10 mg) for 12 h at 37˚C. ROS levels in macrophages were measured using a 2,7-dichlorofluorescin diacetate (DCFH-DA) probe (Beyotime Institute of Biotechnology). Fluorescence microscopy was used to observe the expression of green fluorescence in cells, and the images were captured at a x200 magnification.

Iron oxide nanoparticle association efficiency. The Fe_3O_4 concentration was analyzed using an iron assay kit (Sigma-Aldrich; Merck KGaA). Aliquots of 10 μl of the 100 mM Iron Standard solution were diluted with 990 μl water to generate a 1 mM standard solution. Different amounts of the 1 mM standard solution (0, 2, 4, 6, 8 and 10 μl) were added into a 96-well plate to generate 0, 2, 4, 6, 8 and 10 nmol/well standards at room temperature, respectively. Iron Assay buffer was then added to each well to bring the volume to 100 μl, prior to the addition of 5 μl Iron Reducer to each standard well. Lyophilized powder (10 mg) of CD206-Fe_3O_4-PLGA or Fe_3O_4-PLGA nanoparticles was completely dissolved in 500 μl DMSO. Subsequently, 50 μl this solution was mixed with 50 μl Iron Assay buffer and 5 μl Iron Reducer. A horizontal shaker was used to mix the samples, and the reaction mixture was incubated for 30 min at room temperature, protecting the plate from light during the incubation. Subsequently, 100 μl Iron Probe was added to each well containing standard or test samples. The samples were mixed using a horizontal shaker, and the reaction was allowed to incubate in the dark for 60 min at room temperature. Ultraviolet spectrophotometer (Thermo NanoDrop 3300, Thermo Fisher 012 Scientific, Inc.) was used to determine the absorbance value of each sample at 593 nm. The absorbance values obtained from appropriate iron standards were then used to plot a standard curve, and the concentration of iron was obtained via value conversion. The carrier rate of Fe_3O_4 was determined using the following formula: Carrier rate of Fe_3O_4 (%)=(the mass of Fe_3O_4 in the sample)/(the total mass of added Fe_3O_4) x100%.

Effect of nanoparticles on mouse model. A total of 15 female 6-week-old BALB/c-57 mice weighing 18-22 g were purchased from the Experimental Animal Center of Chongqing Medical University. Full value nutrient granulated feed was used to raise mice, and the feed was added twice a week. The water was supplied by drinking bottle, and the drinking bottle was changed 2-3 times a week. The feeding environment was controlled at 18-22˚C, humidity was 50-60%, and the light/dark cycle was 12:12 h.

Animals received humane care in accordance with the guidelines provided by the Administrative measures of Chongqing Municipality on laboratory animals (order no. 195 of Chongqing Municipal People's Government). The animal protocols used in the present study were evaluated and approved by the Animal Use and Ethics Committee of

The 2nd Affiliated Hospital of Chongqing Medical University (protocol no. 2015-18).

A total of 15 subcutaneous tumorigenic BALB/c-57 mice were randomly divided into three groups (five mice/group). A total of $5x10^6$ murine mammary carcinoma cells (4T1 cell line) were injected subcutaneously on the back of mice. About a week later, the diameter of subcutaneous tumor reached 0.5 cm, and each mouse was given 200 μl PLGA suspension, 200 μl CD206-Fe_3O_4-PLGA suspension or 200 μl ferric citrate solution via tail vein injection once a day for 14 days. All mice were sacrificed by neck dislocation, and the tumor, liver, spleen and lung were removed completely at the end of the experiment.

Determination of iron content in tissues. Subcutaneous tumors, livers, spleens and lungs were harvested from 15 subcutaneous tumorigenic mice. Portions of tissue (1.5 g) were carefully extracted and washed three times in PBS to completely remove the red blood cells. RIPA lysis buffer (5 ml, Beyotime Institute of Biotechnology) was then added, and the tissue samples were ground sufficiently for 20 min with a homogenizer, before the insoluble material was removed via centrifugation (15,000 x g for 10 min at 4˚C). The remaining procedures are the same as those aforementioned for the measurement of iron oxide nanoparticle association efficiency. The absorbance value of control group was used as the control, and the ratio of absorbance value between the experimental and control groups was regarded as the relative iron concentration.

Anti-CD206 antibody conjugation efficiency. Rabbit anti-mouse secondary antibodies (10 μl) to anti-CD206 labeled with TRITC (Abcam) were added to the prepared nanoparticle suspension, and the mixture was incubated for 1 h at 37˚C. The mixture was subsequently centrifuged (15,000 x g for 10 min at 4˚C) to remove the excess secondary antibodies, and then washed three times with PBS. Fluorescence microscopy was used to observe the conjugation of the fluorescent secondary antibodies, and flow cytometry (FACSCalibur; BD Biosciences) was used to detect the carrier rate of anti-CD206 antibodies at room temperature, and without a blocking treatment.

Cell culture. RAW 264.7 cells (mouse monocyte macrophages) and 4T1 cells (murine mammary carcinoma cells) were purchased from the American Type Culture Collection. Cells were cultured in HyClone® DMEM (Thermo Fisher Scientific, Inc.) with 10% FBS containing 1% (v/v) penicillin-streptomycin and 1% (v/v) Fungizone® antimycotic. Cells were maintained in 37˚C humidified air containing 5% CO_2.

$1x10^6$ macrophages were seeded in 6-well plates and cultured with 2 ml medium for 3 h. A total of 2 μl IL-4 (SRP3211-20UG, Sigma-Aldrich; Merck KGaA)was then added into the medium, and the cells were cultured for a further 12 h at 37˚C to obtain high expression levels of CD206 in the macrophages. Macrophages were subsequently incubated at 37˚C with 500 μl CD206-Fe_3O_4-PLGA nanoparticles or with Fe_3O_4-PLGA nanoparticle suspension, for 30 min. Then, the macrophages were washed three times with PBS, incubated with rabbit anti-mouse secondary antibodies labeled with TRITC (1:1,000) at room temperature for 1 h and washed with PBS for a further three times. Fluorescence microscopy was used to observe the targeting capacity of the nanoparticles (magnification, x400).

Effect of nanoparticles on macrophage polarization. $1x10^7$ macrophages were incubated with 2 μl IL-4 for at 37˚C 12 h to obtain macrophages highly expressing CD206. Subsequently, 500 μl CD206-Fe_3O_4-PLGA (10 mg/ml), Fe_3O_4-PLGA (10 mg/ml), PLGA (10 mg/ml) or ferric citrate (1.2 mg/ml) was added into the medium, and the cells were cultured at 37˚C for a further 4 h. Protein and RNA were then harvested from the macrophages.

Reverse transcription-quantitative PCR (RT-qPCR). Total RNA was extracted from the macrophages using TRIzol reagent (Invitrogen; Thermo Fisher Scientific, Inc.) according to the manufacture's protocol. A total of 30 ng RNA/sample was reverse transcribed into cDNA using the PrimeScript™ RT Reagent kit (Takara Biotechnology Co., Ltd. cat. no. RR037A) at 37˚C for 15 min, 85˚C for 5 sec and 4˚C hold. A two-step RT-PCR program (Initial denaturation at 95˚C for 5 sec, followed by the annealing/elongation stage with 40 cycles for 30 sec at 60˚C) was used for amplification with specific primers (Sigma-Aldrich; Merck KGaA). RT-qPCR was performed using SYBR® Green (Takara Biotechnology Co., Ltd.) and the Applied Biosystems ABI Prism 7900 Sequence Detection system (Thermo Fisher Scientific, Inc.). Gene expression was analyzed according to the $2^{-\Delta\Delta Cq}$ method (28), and GAPDH mRNA expression was used as the control.

Western blotting. The concentration of protein was determined using the BCA method. After determining the protein concentration, 200 μl protein sample was mixed with 50 μl buffer and the sample protein was denatured at 100˚C for 10 min. Then, 10% SDS-PAGE was performed with 30 mg aliquots of protein. The obtained PVDF membranes (Beyotime Institute of Biotechnology) were blocked with 5% BSA at room temperature for 60 min and incubated with primary antibodies of TNF-α, IL-1β, Arg1, TGF-β, IL-10 and iNOS (all 1:1,000) overnight at 4˚C. Subsequently, the membranes were incubated with the corresponding secondary antibodies (cat. nos. A0216 and A0208; 1:1,000) at 37˚C for 1 h. The membranes were washed three times with PBS-Tween-20 (0.3% Tween), and then analyzed and scanned using Quantity One software (version 5.2.1; Bio-Rad Laboratories, Inc.) after incubation with an enhanced chemiluminescence reagent (EMD Millipore).

Statistical analysis. All data were analyzed using SPSS 17.0 software (SPSS, Inc.). All experiments were performed in triplicate and data are presented as the mean ± standard deviation. One-way ANOVA followed by Tukey's test were used to compare the parameters among >2 groups. The statistical differences between two groups were determined using unpaired Student's t-test. $P<0.05$ was considered to indicate a statistically significant difference.

Results

Characteristics of nanoparticles. The optical microscopy and scanning electron microscopy analyses identified that the

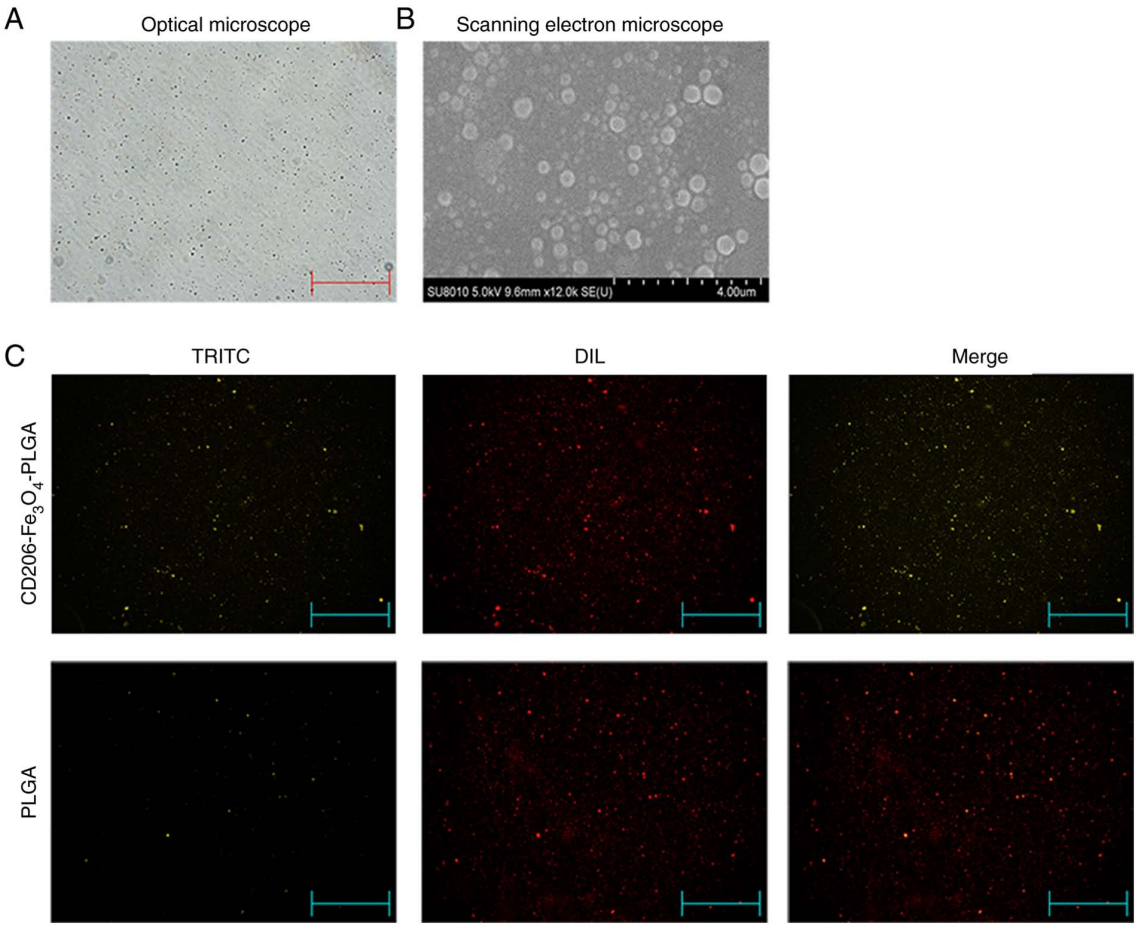

Figure 1. Characteristics of nanoparticles. (A) Nanoparticles observed under an optical microscope (magnification, x100). (B) Scanning electron micrographs of nanoparticles (magnification, x50,000). (C) Nanoparticles were observed under a fluorescence microscope. The red color indicates nanoparticles that were stained with DIL, while the yellow color indicates nanoparticles conjugated with anti-CD206 antibodies (magnification, x100). DIL, DiIC18(3); TRITC, tetramethylrhodamine; PLGA, Poly(lactic-co-glycolic) acid.

nanoparticles had a relatively uniform particle size, a spherical, smooth surface and a good dispersion (Fig. 1A and B). Fluorescence microscopy indicated that the anti-CD206 antibody labeled with TRITC was successfully conjugated with PLGA nanoparticles, and all the PLGA nanoparticles were labeled with DIL (Fig. 1C). The particle size of nanoparticles were 260-295 nm, and the ζ potential values were -19 to -33 mv. The Fe_3O_4 association efficiency ranged from 65-75%, and the anti-CD206 conjunction efficiency ranged from 65-70% (Table II). It shows that the nanoparticles had a uniform particle size, good dispersion in aqueous solution, good Fe_3O_4 association efficiency and anti-CD206 conjunction efficiency.

Selective enhancement of the intra-tumoral iron level. Our previous study reported that body iron concentration at a high level in mice may inhibit tumor growth by promoting M1 polarization in TAMs (29). Subsequent experimental results in the present study demonstrated that tail vein injection of ferric citrate in mice could significantly increase the iron content in the liver, spleen and lung compared with the saline group (Fig. 2A), which may lead to potential organ damage. RAW 264.7 cells were pretreated with IL-4 to obtain M2 macrophages, as TAM cells, which express high levels of CD206. CD206-Fe_3O_4-PLGA nanoparticles were used to transport Fe_3O_4 to CD206-positive macrophages. Compared with the control group, CD206-Fe_3O_4-PLGA significantly increased the iron content in macrophages (Fig. 2B). Fluorescence assay results demonstrated that the CD2060-positive macrophages (i.e., M2 macrophages) exhibited a stronger PLGA-binding capability in the CD206-Fe_3O_4-PLGA group after 30 min co-culture, while the CD206-negative macrophages (M0/M1 macrophages) did not have a strong binding ability (Fig. 2C and D).

Promoting macrophage polarization and cellular ROS production. Western blotting and RT-qPCR were used to assess whether nanoparticles could promote the polarization of macrophages. Western blot and RT-qPCR analyses demonstrated that CD206-Fe_3O_4-PLGA significantly promoted the expression of TNF-α, IL-1β and iNOS ($P<0.05$), but inhibited the expression of TGF-β, IL-10 and Arg1 ($P<0.05$; Fig. 3A and B). The results of these experiments demonstrated that CD206-Fe_3O_4-PLGA and Fe_3O_4-PLGA nanoparticles promoted M1 polarization of the macrophages. Furthermore, it was found that the PLGA nanoparticles alone were not able to promote macrophage polarization.

Pretreatment of the CD206-Fe_3O_4-PLGA and Fe_3O_4-PLGA nanoparticles with IL-4 resulted in increased ROS production in macrophages with elevated intracellular iron content

Table II. Characteristics of the NPs.

Formula	Mean effective diameter (nm)	ζ potential (mV)	Anti-CD206 conjugation efficiency (%)	Fe_3O_4 association efficiency (%)
PLGA NPs	261.4±22.5	-25.6±4.4	-	-
Fe_3O_4-PLGA	283.8±24.1	-27.3±5.7	-	75.3±5.2
CD206-Fe_3O_4-PLGA	294.3±17.8	-32.2±3.5	67.8±2.5	66.7±3.7

PLGA, poly(lactic-co-glycolic) acid; NP, nanoparticle.

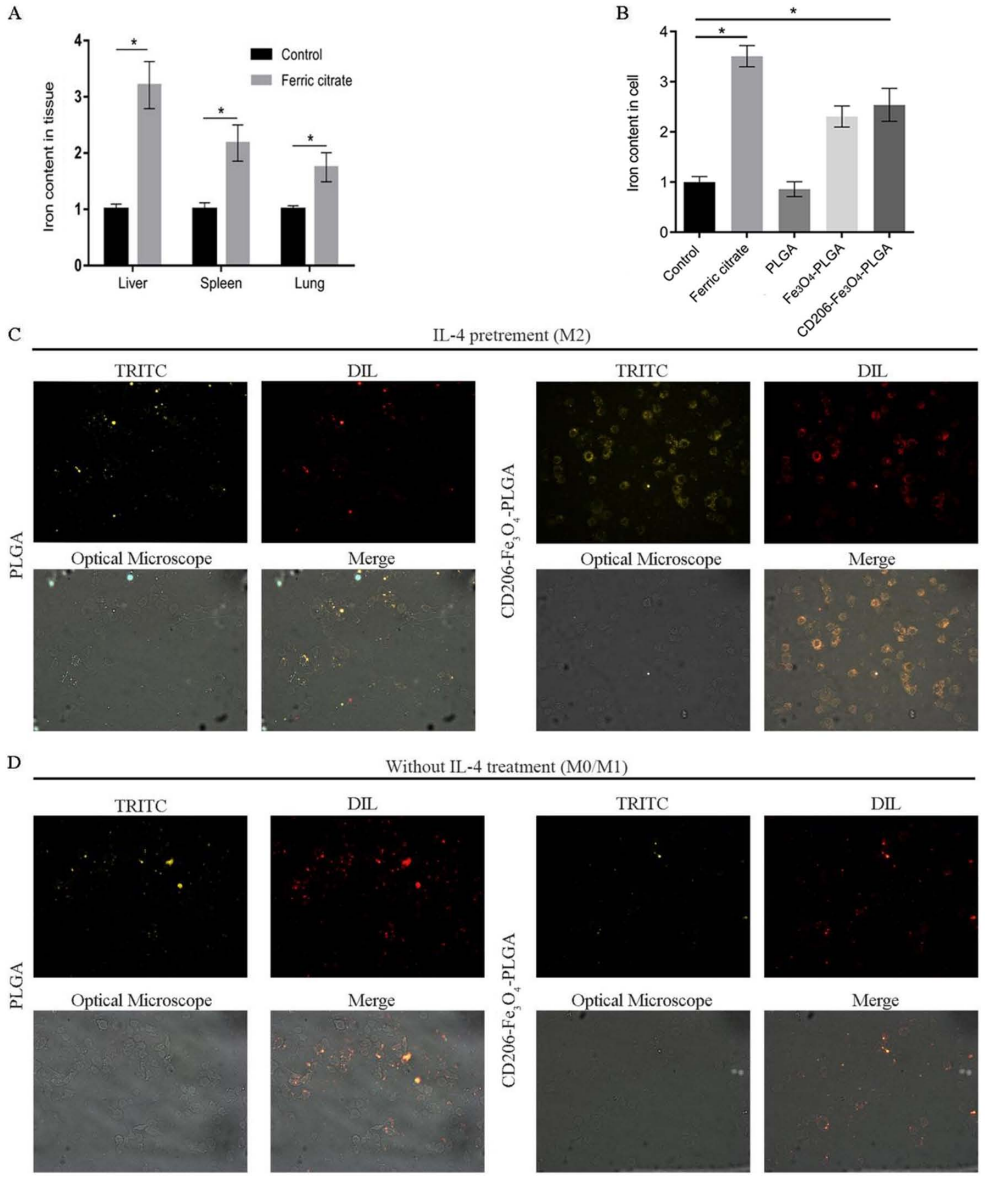

Figure 2. Selective enhancement of the intra-tumoral iron level. (A) Mice injected with ferric citrate had a higher relative iron content in their liver, spleen, lung and subcutaneous tumor compared with the control group. (B) Compared with the control group, the relative iron content of macrophages, pretreated with IL-4 and co-cultured with iron and CD206-Fe_3O_4-PLGA for 24 h, was increased significantly ($^*P<0.05$), but not in the group co-culture with PLGA alone. (C) Immunofluorescence analysis demonstrated that a large number of CD206-Fe_3O_4-PLGA nanoparticles surrounded the macrophages pretreated with IL-4 compared with the PLGA group (magnification, x400). (D) Immunofluorescence analysis demonstrated that only a few PLGA and CD206-Fe_3O_4-PLGA nanoparticles surrounded the macrophages without IL-4 pretreatment (magnification, x400). PLGA, poly(lactic-co-glycolic) acid; DIL, DiIC18(3); TRITC, tetramethylrhodamine.

identified via DCFH-DA, a probe used for detecting ROS in living cells (Fig. 3C).

Nanoparticles promote M1 polarization of TAMs in an established mouse model. Tumor-bearing mice were injected with

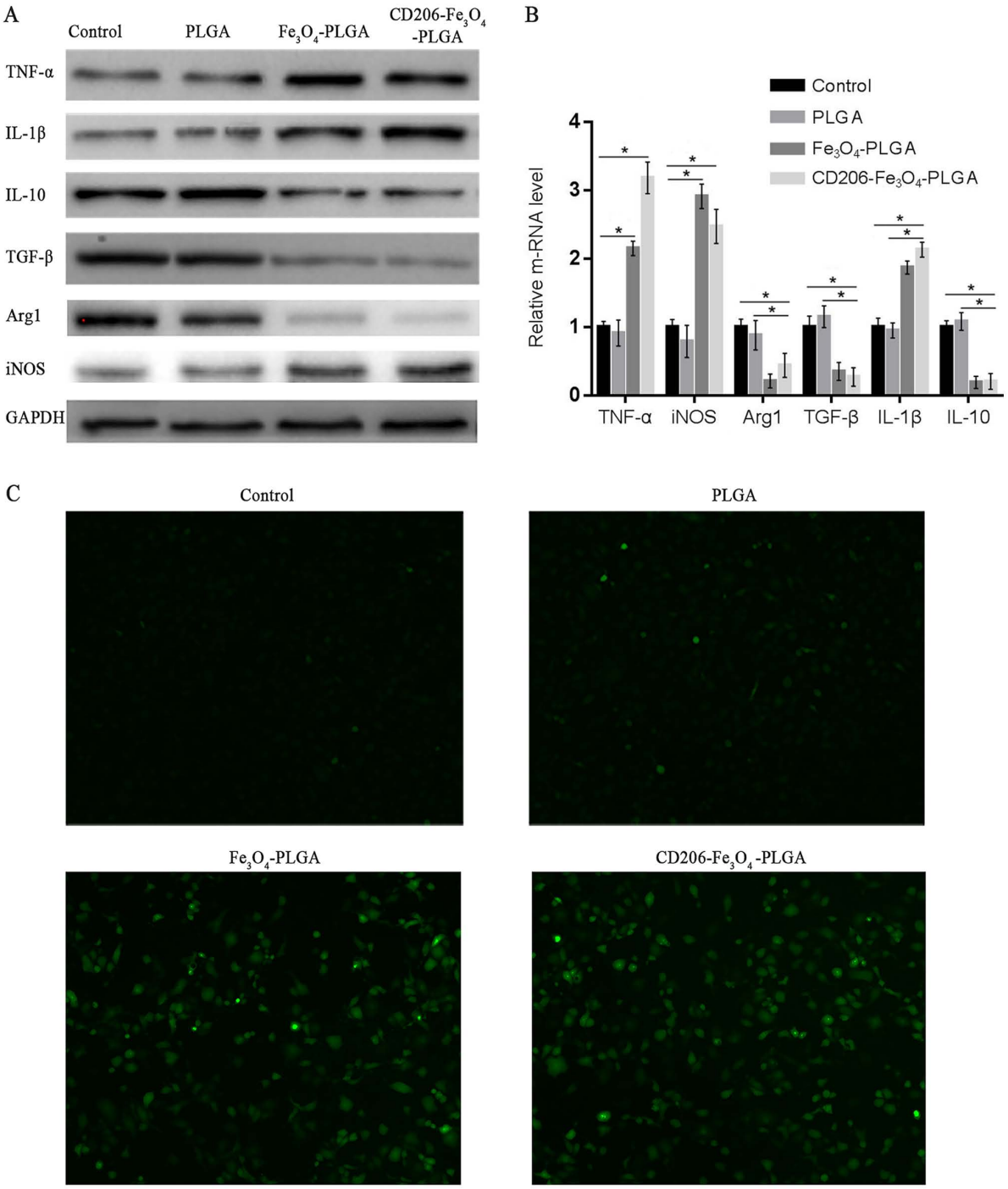

Figure 3. Promoting macrophage polarization and cellular ROS production. (A) Western blotting and (B) reverse transcription-quantitative PCR results indicated that CD206-Fe_3O_4-PLGA promoted the expression levels of TNF-α, IL-1β and iNOS (*P<0.05), while the expression levels of TGF-β, IL-10 and Arg1 were inhibited (*P<0.05). (C) A reactive oxygen probe assay demonstrated that PLGA did not significantly increase intracellular ROS, but an enhanced level of ROS production was observed in macrophages treated with CD206-Fe_3O_4-PLGA and Fe_3O_4-PLGA (magnification, x100). ROS, reactive oxygen species; iNOS, inducible nitric oxide synthase; PLGA, poly(lactic-co-glycolic) acid; Arg1, Arginase 1.

CD206-Fe_3O_4-PLGA, Fe_3O_4-PLGA, PLGA nanoparticles or ferric citrate via the tail vein in order to study the targeting properties of nanoparticles *in vivo*. An immunofluorescence assay was subsequently used to observe the deposition of nanoparticles in tumor tissues. The results indicated that there were increased numbers of CD206-Fe_3O_4-PLGA nanoparticles in the subcutaneous tissue compared with PLGA nanoparticles (Fig. 4A).

Double-labeled tissue fluorescence was used to detect the polarization of macrophages in tumor tissues. It was identified that macrophages in the CD206-Fe_3O_4-PLGA group expressed a higher level of CD86, a specific marker of the M1 subtype (Fig. 4B). The diameter of subcutaneous tumor of mice treated with PLGA microspheres was smaller compared with control and PLGA groups (both P<0.05; Fig. 4C and D). The tumor tissue of the CD206-Fe_3O_4-PLGA group contained a higher iron concentration, whereas the liver and spleen contained less iron, compared with the ferric citrate group (P<0.05; Fig. 4E).

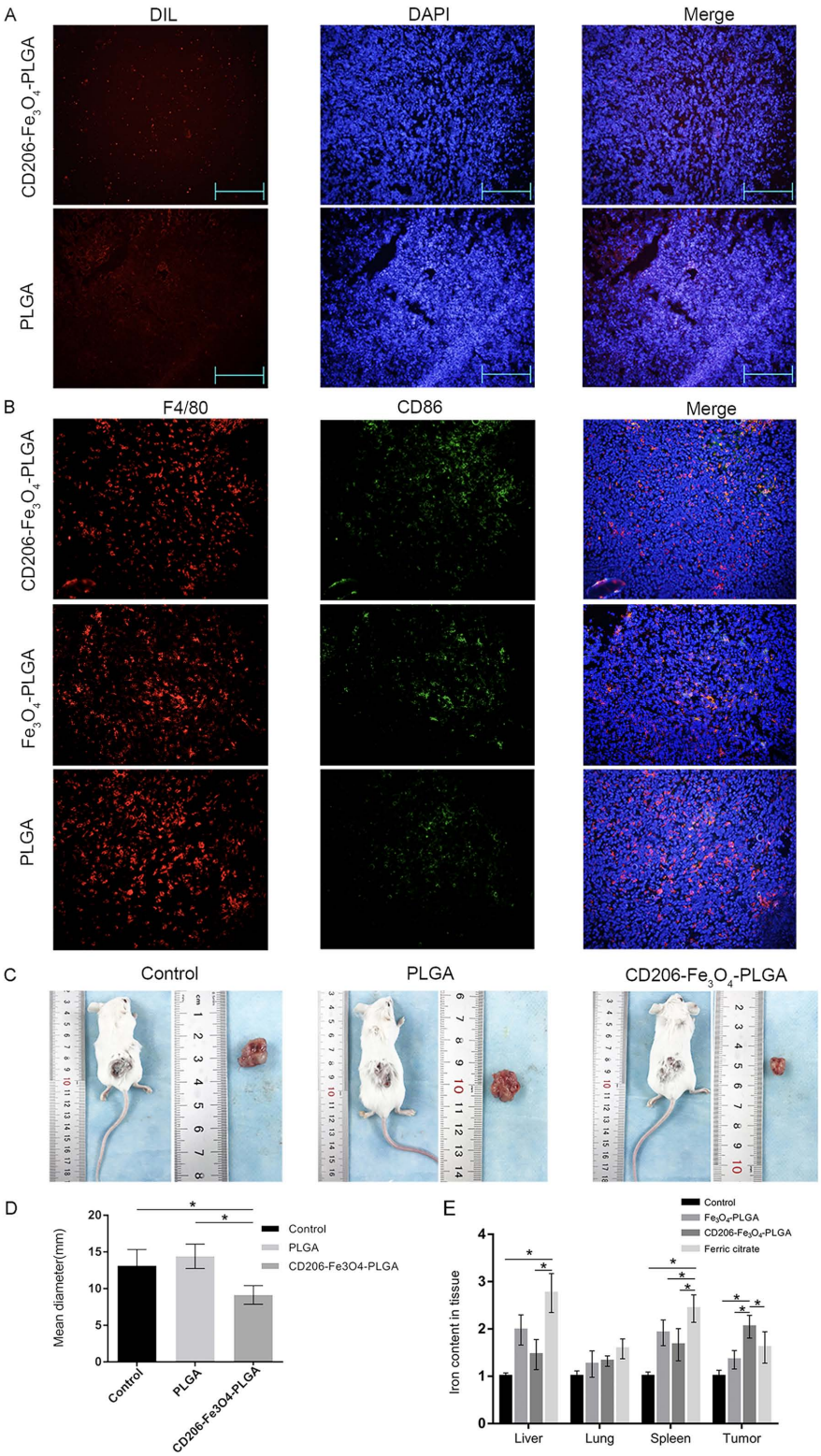

Figure 4. Nanoparticles slow down the growth of subcutaneous tumors in mice. (A) Immunofluorescence assay results indicated that there were more nanoparticles in the subcutaneous tissue of the CD206-Fe_3O_4-PLGA treatment group compared with the PLGA group (magnification, x100). (B) Immunofluorescence assay results demonstrated that the expression of CD86 was higher in TAMs treated with CD206-Fe_3O_4-PLGA nanoparticles compared with the control and Fe_3O_4-PLGA groups. (C) Representative tumor images. (D) CD206-Fe_3O_4-PLGA-treated mice exhibited subcutaneous tumors that had a smaller diameter compared with the other groups (*P<0.05). (E) Compared with the ferric citrate group, there was a higher relative iron content in the subcutaneous tumor tissue of the CD206-Fe_3O_4-PLGA treatment group, but smaller concentration in the liver and spleen (*P<0.05). TAM, tumor-associated macrophage; PLGA, poly(lactic-co-glycolic) acid.

Discussion

TAMs may be associated with up to 50% of the total tumors, and often associated with a poor patient prognosis (30). Therefore, TAM ablation (or TAM reprogramming) has become a potential antitumor treatment strategy.

M1 macrophages cannot only inhibit tumor cells via secretion and phagocytosis, but can also block DNA replication of

tumor cells by absorbing and sequestering the iron found in the microenvironment (31). M2 macrophages are major sites for taking up, metabolizing, storing and exporting iron (31). M2 macrophages can release intracellular iron ions and promote iron internalization and sequestration via known receptors, such as megalin, contributing to cancer cell survival and metastasis (32). Large numbers of iron ions are required for the growth and proliferation of tumor cells (33-35). Therefore, the introduction or elimination of iron in cells to destroy the homeostasis of iron metabolism has become a potential avenue for cancer treatment.

Iron chelators are able to both effectively decrease the content of iron in tumor cells and inhibit the proliferation of aggressive tumors, leading to G_1/S cell cycle arrest and apoptosis (36,37). Although iron chelators do exert therapeutic effects on tumors, their side effects cannot be ignored. Iron chelators have been reported to activate the hypoxia-inducible factor-1α pathway, and induce the expression levels of urokinase plasminogen activator and MMP-2, resulting in enhanced metastasis via degrading the extracellular matrix and increasing the level of VEGF, leading to toxic anemia and edema (38-41).

Iron oxide nanoparticles (IONPs) have been widely used for drug targeting and diagnostic applications (42). The concentration of intracellular iron in dendritic cells can be increased by co-culturing with IONPs; however, previous studies have revealed that an increase of iron concentration in dendritic cells exerts little influence on the phenotype and maturation of dendritic cells (43,44). SPION treatment has been reported to produce ROS and activate the extracellular signal-regulated kinase and AKT pathways (45). Moreover, SPION leads to impaired chemotactic migration and an increased invasive capacity of M2 macrophages, but does not activate either the c-Jun terminal kinase or the p38-mitogen-activated protein kinase pathways (45). It has been shown that IONPs induce differential effects on antigen-specific cytokine expression mediated by T cells, in which IFN-γ expression is sensitized, while the effect on IL-4 expression is refractory (46). In addition, the suppressive effect of IONPs on IRN-γ is closely associated with a decrease in the level of glutathione (46).

It has been reported that exogenous administration of iron nitrate leads to deposition of most iron in the liver and spleen, and only a fraction of the hemosiderin-laden macrophages were observed in the mammary tumors (47).

PLGA particles have been revealed to encapsulate SPIONs and BSA, and the significantly improved uptake of BSA/SPION-PLGA particles into RAW 264.7 cells is observed under the influence of an external magnetic field compared with the uptake of particles without an external magnetic field (48). These particles are shown to significantly enhance bone marrow-derived dendritic cell maturation by upregulating the expression levels of major histocompatibility complex II, CD80 and CD86 (48).

In the present study, CD206 monoclonal antibody-conjugated nanoparticles were able to specifically bind to the surface of CD206-positive cells when circulating in the blood vessels. Collectively, the current results demonstrated that the nanoparticles could specifically bind to M2 macrophages *in vivo* and *in vitro*. After being phagocytized by the TAMs, the nanoparticles were gradually hydrolyzed, releasing Fe_3O_4, which was degraded into iron ions in the lysosomes, thus increasing the intracellular concentration of iron in the macrophages and inducing reprogramming of the M2 macrophages.

In conclusion, the present study demonstrated that CD206-Fe_3O_4-PLGA nanoparticles were successfully constructed to increase the iron content in M2 macrophages, thus promoting the repolarization of M2 macrophages to the M1 subtype. This effect lead to an inhibition of the growth of tumors, and also decreased the deposition of physiological tissue iron. Therefore, the present study provided a potential approach for tumor immunotherapy; however, most targeted therapies are not aimed at a specific type of cells. Thus, in a follow-up study, further methods to improve the targeting ability, such as identifying additional unique cell markers or coupling two or more specific antibodies, will be developed.

Acknowledgements

Not applicable.

Funding

The present study was supported by the National Natural Science Foundation of China (grant nos. 81470899 and 81170442) and the Talent Project of The Second Affiliated Hospital of Chongqing Medical University (grant no. 2016).

Availability of data and materials

All data generated or analyzed during this study are included in this published article.

Authors' contributions

YZ and KTQ acquired, analyzed and interpreted the data, and drafted the initial manuscript. HMT and PZ acquired, analyzed and interpreted the data. QMF and ZJL conceived the present study and designed the experiments, and analyzed and interpreted the data. ZJL also helped draft the initial manuscript and revise it for intellectual content. All authors read and approved the final manuscript.

Ethics approval and consent to participate

All animal experiments were approved by the Animal Use and Ethics Committee of The 2nd Affiliated Hospital of Chongqing Medical University (approval no. 2015-18).

Patient consent for publication

Not applicable.

Competing interests

The authors declare that they have no competing interests.

References

1. Juhas U, Ryba-Stanisławowska M, Szargiej P and Myśliwska J: Different pathways of macrophage activation and polarization. Postepy Hig Med Dosw (Online) 69: 496-502, 2015.
2. Jung M, Mertens C and Brüne B: Macrophage iron homeostasis and polarization in the context of cancer. Immunobiology 220: 295-304, 2015.

3. Chlosta S, Fishman DS, Harrington L, Johnson EE, Knutson MD, Wessling-Resnick M and Cherayil BJ: The iron efflux protein ferroportin regulates the intracellular growth of Salmonella enterica. Infect Immun 74: 3065-3067, 2006.
4. Paradkar PN, De Domenico I, Durchfort N, Zohn I, Kaplan J and Ward DM: Iron depletion limits intracellular bacterial growth in macrophages. Blood 112: 866-874, 2008.
5. Recalcati S, Locati M, Gammella E, Invernizzi P and Cairo G. Iron levels in polarized macrophages: Regulation of immunity and autoimmunity. Autoimmun Rev 11: 883-889, 2012.
6. Lewin M, Carlesso N, Tung CH, Tang XW, Cory D, Scadden DT and Weissleder R: Tat peptide-derivatized magnetic nanoparticles allow in vivo tracking and recovery of progenitor cells. Nat Biotechnol 18: 410-414, 2000.
7. Namdeo M, Saxena S, Tankhiwale R, Bajpai M, Mohan YM and Bajpai SK: Magnetic nanoparticles for drug delivery applications. J Nanosci Nanotechnol 8: 3247-3271, 2008.
8. Zanganeh S, Hutter G, Spitler R, Lenkov O, Mahmoudi M, Shaw A, Pajarinen JS, Nejadnik H, Goodman S, Moseley M, *et al*: Iron oxide nanoparticles inhibit tumour growth by inducing pro-inflammatory macrophage polarization in tumour tissues. Nat Nanotechnol 11: 986-994, 2016.
9. Thorek DL, Chen AK, Czupryna J and Tsourkas A: Superparamagnetic iron oxide nanoparticle probes for molecular imaging. Ann Biomed Eng 34: 23-38, 2006.
10. Laskar A, Eilertsen J, Li W and Yuan X: SPION primes THP1 derived M2 macrophages towards M1-like macrophages. Biochem Biophys Res Commun 441: 737-742, 2013.
11. Astete C and Sabliov CM: Synthesis and characterization of PLGA nanoparticles. J Biomater Sci Polym Ed 17: 247-289, 2006.
12. Kapoor DN, Bhatia A, Kaur R, Sharma R, Kaur G and Dhawan S: PLGA: A unique polymer for drug delivery. Ther Deliv 6: 41-58, 2015.
13. Postlethwait RW: Polyglycolic acid surgical suture. Arch Surg 101: 489-494, 1970.
14. Khatri K, Goyal A and Vyas S: Potential of nanocarriers in genetic immunization. Recent Pat Drug Deliv Formul 2: 68-82, 2008.
15. Byrne JD, Betancourt T and Brannon-Peppas L: Active targeting schemes for nanoparticle systems in cancer therapeutics. Adv Drug Deliv Rev 60: 1615-1626, 2008.
16. Gu F, Zhang L, Teply BA, Mann N, Wang A, Radovic-Moreno AF, Langer R and Farokhzad OC: Precise engineering of targeted nanoparticles by using self-assembled biointegrated block copolymers. Proc Natl Acad Sci USA 105: 2586-2591, 2008.
17. Maeda H: Tumor-selective delivery of macromolecular drugs via the EPR effect: Background and future prospects. Bioconjugate Chem 21: 797-802, 2010.
18. Xu X, Ho W, Zhang X, Bertrand N and Farokhzad O: Cancer nanomedicine: From targeted delivery to combination therapy. Trends Mol Med 21: 223-232, 2015.
19. Wang G, Griffin JI, Inturi S, Brenneman B, Banda NK, Holers VM, Moghimi SM and Simberg D: In vitro and in vivo differences in murine third complement component (C3) opsonization and macrophage/leukocyte responses to antibody-functionalized iron oxide nanoworms. Front Immunol 8: 151, 2017.
20. Jokerst JV, Lobovkina T, Zare RN and Gambhir SS: Nanoparticle PEGylation for imaging and therapy. Nanomedicine (Lond) 6: 715-728, 2011.
21. Kwon IK, Lee SC, Han B and Park K: Analysis on the current status of targeted drug delivery to tumors. J Controlled Release 164: 108-114, 2012.
22. Ruenraroengsak P, Cook JM and Florence AT: Nanosystem drug targeting: Facing up to complex realities. J Control Release 141: 265-276, 2010.
23. Badkas A, Frank E, Zhou Z, Jafari M, Chandra H, Sriram V, Lee JY and Yadav JS: Modulation of in vitro phagocytic uptake and immunogenicity potential of modified Herceptin®-conjugated PLGA-PEG nanoparticles for drug delivery. Colloids Surf B Biointerfaces 162: 271-278, 2018.
24. Allen TM: Ligand-targeted therapeutics in anticancer therapy. Nat Rev Cancer 2: 750-763, 2002.
25. Peer D, Karp JM, Hong S, Farokhzad OC, Margalit R and Langer R: Nanocarriers as an emerging platform for cancer therapy. Nat Nanotechnol 2: 751-760, 2007.
26. Kamaly N, Yameen B, Wu J and Farokhzad OC: Degradable controlled-release polymers and polymeric nanoparticles: Mechanisms of controlling drug release. Chem Rev 116: 2602-2663, 2016.
27. Moura CC, Segundo MA, Neves Jd, Reis S and Sarmento B: Co-association of methotrexate and SPIONs into anti-CD64 antibody-conjugated PLGA nanoparticles for theranostic application. Int J Nanomedicine 9: 4911-4922, 2014.
28. Livak KJ and Schmittgen TD: Analysis of relative gene expression data using real-time quantitative PCR and the 2(-Delta Delta C(T)) method. Methods 25: 402-408, 2001.
29. Zhou Y, Que KT, Zhang Z, Yi ZJ, Zhao PX, You Y, Gong JP and Liu ZJ: Iron overloaded polarizes macrophage to proinflammation phenotype through ROS/acetylp53 pathway. Cancer Med 7: 4012-4022, 2018.
30. DeNardo DG, Brennan DJ, Rexhepaj E, Ruffell B, Shiao SL, Madden SF, Gallagher WM, Wadhwani N, Keil SD, Junaid SA, *et al*: Leukocyte complexity predicts breast cancer survival and functionally regulates response to chemotherapy. Cancer Discov 1: 54-67, 2011.
31. Wang Y, Yu L, Ding J and Chen Y: Iron metabolism in cancer. Int J Mol Sci 20: 95, 2018.
32. Duan X, He K, Li J, Cheng M, Song H, Liu J and Liu P. Tumor associated macrophages deliver iron to tumor cells via Lcn2. Int J Physiol Pathophysiol Pharmacol 10: 105-114, 2018.
33. Pinnix ZK, Miller LD, Wang W, D'Agostino R Jr, Kute T, Willingham MC, Hatcher H, Tesfay L, Sui G, Di X, *et al*: Ferroportin and iron regulation in breast cancer progression and prognosis. Sci Transl Med 2: 43ra56, 2010.
34. Majewska U, Banaś D, Braziewicz J, Góźdź S, Kubala-Kukuś A and Kucharzewski M: Trace element concentration distributions in breast, lung and colon tissues. Phys Med Biol 52: 3895-3911, 2007.
35. Torti SV and Torti FM: Iron and cancer: More ore to be mined. Nat Rev Cancer 13: 342-355, 2013.
36. Shen L, Zhao HY, Du J and Wang F: Anti-tumor activities of four chelating agents against human neuroblastoma cells. In Vivo 19: 233-236, 2005.
37. Li P, Zheng X, Shou K, Niu Y, Jian C, Zhao Y, Yi W, Hu X and Yu A: The iron chelator Dp44mT suppresses osteosarcoma's proliferation, invasion and migration: In vitro and in vivo. Am J Transl Res 8: 5370-5385, 2016.
38. Tsai SH, Huang PH, Hsu YJ, Peng YJ, Lee CH, Wang JC, Chen JW and Lin SJ: Inhibition of hypoxia inducible factor-1α attenuates abdominal aortic aneurysm progression through the down-regulation of matrix metalloproteinases. Sci Rep 6: 28612, 2016.
39. Kontoghiorghes GJ: Ethical issues and risk/benefit assessment of iron chelation therapy: Advances with deferiprone/deferoxamine combinations and concerns about the safety, efficacy and costs of deferasirox. Hemoglobin 32: 1-15, 2008.
40. Di Nicola M, Barteselli G, Dell'Arti L, Ratiglia R and Viola F: Functional and structural abnormalities in deferoxamine retinopathy: A review of the literature. Biomed Res Int 2015: 249617, 2015.
41. Hamilton JL, Hatef A, Imran ul-Haq M, Nair N, Unniappan S and Kizhakkedathu JN: Clinicallyapproved iron chelators influence zebrafish mortality, hatching morphology and cardiac function. PLoS One 9: e109880, 2014.
42. Xie J, Huang J, Li X, Sun S and Chen X: Iron oxide nanoparticle platform for biomedical applications. Curr Med Chem 16: 1278-1294, 2009.
43. Mou Y, Chen B, Zhang Y, Hou Y, Xie H, Xia G, Tang M, Huang X, Ni Y and Hu Q: Influence of synthetic superparamagnetic iron oxide on dendritic cells. Int J Nanomedicine 6: 1779-1786, 2011.
44. Verdijk P, Scheenen TW, Lesterhuis WJ, Gambarota G, Veltien AA, Walczak P, Scharenborg NM, Bulte JWM, Punt CJA, Heerschap A, *et al*: Sensitivity of magnetic resonance imaging of dendritic cells for in vivo tracking of cellular cancer vaccines. Int J Cancer 120: 978-984, 2006.
45. Rojas JM, Sanz-Ortega L, Mulens-Arias V, Gutiérrez L, Pérez-Yagüe S and Barber DF: Superparamagnetic iron oxide nanoparticle uptake alters M2 macrophage phenotype, iron metabolism, migration and invasion. Nanomedicine 12: 1127-1138, 2016.
46. Shen CC, Liang HJ, Wang CC, Liao MH and Jan TR: A role of cellular glutathione in the differential effects of iron oxide nanoparticles on antigen-specific T cell cytokine expression. Int J Nanomedicine 6: 2791-2798, 2011.
47. Leftin A, Ben-Chetrit N, Klemm F, Joyce JA and Koutcher JA: Iron imaging reveals tumor and metastasis macrophage hemosiderin deposits in breast cancer. PLoS One 12: e0184765, 2017.
48. Saengruengrit C, Ritprajak P, Wanichwecharungruang S, Sharma A, Salvan G, Zahn DRT and Insin N: The combined magnetic field and iron oxide-PLGA composite particles: Effective protein antigen delivery and immune stimulation in dendritic cells. J Colloid Interface Sci 520: 101-111, 2018.